Available online at www.sciencedirect.com

ScienceDirect

Geochimica et Cosmochimica Acta 219 (2017) 44–56

Geochimica et Cosmochimica Acta

www.elsevier.com/locate/gca

Effect of Ca content on equilibrium Ca isotope fractionation between orthopyroxene and clinopyroxene

Wenzhong Wang [a,b], Chen Zhou [c], Tian Qin [a,b], Jin-Ting Kang [c], Shichun Huang [d], Zhongqing Wu [a,b,*], Fang Huang [c,*]

[a] *Laboratory of Seismology and Physics of Earth's Interior, School of Earth and Space Sciences, University of Science and Technology of China, Hefei, Anhui 230026, China*

[b] *National Geophysical Observatory at Mengcheng, University of Science and Technology of China, China*

[c] *CAS Key Laboratory of Crust-Mantle Materials and Environments, School of Earth and Space Sciences, University of Science and Technology of China, Hefei, Anhui 230026, China*

[d] *Department of Geoscience, University of Nevada, Las Vegas, NV 89154, United States*

Received 27 April 2017; accepted in revised form 10 September 2017; Available online 19 September 2017

Abstract

Concentration effect on equilibrium inter-mineral isotope fractionation is ubiquitous in solid solution systems, but it is not clear in which concentration range such effect is prominent. Using first-principles calculations, we examine the effect of Ca and Fe contents in orthopyroxene (opx) on its average Ca—O bond length and the equilibrium Ca isotope fractionation factor ($10^3\ln\alpha$) between opx and clinopyroxene (cpx). Our results reveal that the average Ca—O bond length in opx is much smaller than that in cpx and it does not change with variable Ca content x (x and y are mole ratios in $Ca_xFe_yMg_{1-x-y}SiO_3$ thereafter here) when $x \leq 1/48$. Incorporation of Fe ($y \geq 1/32$) into opx with a fixed Ca content can only slightly increase the average Ca—O bond length. $10^3\ln\alpha_{opx\text{-}cpx}$ of $^{44}Ca/^{40}Ca$ is linearly correlated with the average Ca—O bond length in opx, suggesting that $10^3\ln\alpha_{opx\text{-}cpx}$ of $^{44}Ca/^{40}Ca$ is controlled by opx Ca—O bond strength. Our calculations indicate that the Ca concentration effect on $10^3\ln\alpha_{opx\text{-}cpx}$ is significant when x in opx ranges from 2/16 to 1/48, while Fe in natural opx only causes a slight decrease in $10^3\ln\alpha_{opx\text{-}cpx}$.

Our results provide insights into Ca isotope fractionation in high-temperature geochemical processes. Given that Ca content x in opx from natural peridotites is usually lower than 1/32 and Fe content y is generally ~10 mol%, Ca and Fe concentration effects on $10^3\ln\alpha_{opx\text{-}cpx}$ in natural samples are negligible. Rather, $10^3\ln\alpha_{opx\text{-}cpx}$ is mainly controlled by temperature. $10^3\ln\alpha_{opx\text{-}cpx}$ of $^{44}Ca/^{40}Ca$ decreases from 0.50‰ to 0.26‰ when temperature increases from 1000 K to 1400 K if the Fe effect is taken into account. Therefore, if Ca isotope fractionation between opx and cpx ($\Delta^{44/40}Ca_{opx\text{-}cpx}$) in natural peridotites is greater than 0.50‰ or lower than 0.26‰, it may indicate disequilibrium of Ca isotopes. Finally, the large $10^3\ln\alpha_{opx\text{-}cpx}$ relative to our current analytical precision suggests that $\Delta^{44/40}Ca_{opx\text{-}cpx}$ can be used as an independent thermometer with a precision comparable to elemental thermometers. Because most naturally occurring minerals are solid solutions with variable chemical compositions, this study presents a guideline to explore the concentration effect on equilibrium isotope fractionation among minerals.

Keywords: First-principle calculations; Equilibrium fractionation; Ca isotopes; Opx and cpx

* Corresponding authors at: Laboratory of Seismology and Physics of Earth's Interior, School of Earth and Space Sciences, University of Science and Technology of China, Hefei, Anhui 230026, China (Z. Wu) and CAS Key Laboratory of Crust-Mantle Materials and Environments, School of Earth and Space Sciences, University of Science and Technology of China, Hefei, Anhui 230026, China (F. Huang).

E-mail addresses: wuzq10@ustc.edu.cn (Z. Wu), fhuang@ustc.edu.cn (F. Huang).

https://doi.org/10.1016/j.gca.2017.09.022

0016-7037/

1. INTRODUCTION

Calcium has six stable isotopes (^{40}Ca, ^{42}Ca, ^{43}Ca, ^{44}Ca, ^{46}Ca, and ^{48}Ca) with a 20% range in relative mass, which is only smaller than hydrogen and helium in the periodic table. This makes Ca isotopes an important tracer in both cosmochemistry and geochemistry. Calcium isotopes have been applied widely to fundamental geochemical processes, such as the origin and the evolution of the early Solar system, and the formation of the terrestrial planets (Simon et al., 2009; Simon and DePaolo, 2010; Huang et al., 2012; Valdes et al., 2014; Huang and Jacobsen, 2017; Amsellem et al., 2017). Calcium isotopes can also be used to trace the recycling of surface materials into the mantle, such as carbonates (Zhu and Douglas Macdougall, 1998; DePaolo, 2004; Kasemann et al., 2005; Steuber and Buhl, 2006; Jacobson and Holmden, 2008; Holmden, 2009; Huang et al., 2011). The Ca isotopic composition of the bulk Earth is essential in these applications.

It is critical to understand fractionation mechanisms of Ca isotopes between Ca-bearing minerals. Ca isotope data are defined as: $\delta^{44/40}Ca = [(^{44}Ca/^{40}Ca)_{Sample}/(^{44}Ca/^{40}Ca)_{SRM\text{-}915a} - 1] \times 1000‰$ (Halicz et al., 1999). Since SRM915a is now out of stock, it has been replaced by SRM915b in recent studies (e.g. Valdes et al., 2014; Amsellem et al., 2017). Orthopyroxene (opx) and clinopyroxene (cpx) are two major hosts of Ca in the upper mantle. Large Ca isotopic variations of two important Ca-bearing minerals in the mantle (opx and cpx) have been reported (Huang et al., 2010; Kang et al., 2016; Zhao et al., 2017). The Ca isotope offsets between opx and cpx from mantle xenoliths ($\Delta^{44/40}Ca_{opx\text{-}cpx} = \delta^{44/40}Ca_{opx} - \delta^{44/40}Ca_{cpx}$) range from −0.49‰ to 1.11‰ (Huang et al., 2010; Kang et al., 2016; Zhao et al., 2017). Previous Mg isotope studies have suggested that stable isotopes in mantle peridotites can be affected by later metasomatic processes (Young et al., 2009, 2015; An et al., 2017). More recently, the large $\Delta^{44/40}Ca_{opx\text{-}cpx}$ (−0.49‰ to −0.31‰) observed in Yangyuan peridotites have also been explained as disequilibrium isotope fractionation (Zhao et al., 2017). Thus, for better application of Ca isotopes into the study of high-temperature geochemical processes, it is necessary to evaluate equilibrium fractionation of Ca isotopes between opx and cpx.

Most naturally occurring rock-forming minerals, such as olivine, spinel, garnet, pyroxene, feldspar, and amphibole, form solid solutions with large compositional variations. For example, Ca and Fe atoms can replace Mg atoms in opx, cpx, and olivine; and garnet has a large Al content variation. Under thermodynamic equilibrium, compositional variations in solid solutions can be used as thermometers and barometers, such as two-feldspar thermometers, two-pyroxene thermometers and barometers, and silica activity barometer (e.g. Brown and Parsons, 1981; Brey and Köhler, 1990; Beattie, 1993; Benisek et al., 2004; Anderson et al., 2008; Putirka, 2008, 2016). The co-existing opx-cpx pair is also an important geothermometer in the field of igneous petrology (Putirka, 2008, 2016 and references therein).

Although it has been well accepted that chemical compositions of minerals can modify crystal structures and elemental partitioning (Lundstrom et al., 1998; Hill et al., 2000), their effect on inter-mineral stable isotope fractionation has not been fully recognized. Based on first-principles calculations, Feng et al. (2014) revealed that equilibrium Ca isotope fractionation between opx and cpx ($10^3\ln\alpha_{opx\text{-}cpx}$) is not only controlled by temperature, but also by Ca content in opx because average Ca—O bond length in opx is strongly dependent on its Ca content. Specially, when Ca content x in opx ($Ca_xFe_yMg_{1-x-y}SiO_3$) decreases from 1/16 to 1/32, $10^3\ln\alpha_{opx\text{-}cpx}$ increases significantly from 0.19‰ to 0.37‰ at 1273 K, suggesting that the Ca concentration effect can explain the large $\Delta^{44/40}Ca_{opx\text{-}cpx}$ (0.36–0.75‰) observed in San Carlos and Kilbourne Hole peridotites (Huang et al., 2010). Although this theoretical study on opx-cpx system illustrated the controlling factors of inter-mineral equilibrium Ca isotope fractionations and found the upper limit of Ca concentration effect (Feng et al., 2014), there are still two critical issues requiring further exploration.

First, Feng et al. (2014) estimated the upper limit of Ca content in opx beyond which the concentration effect on $10^3\ln\alpha_{opx\text{-}cpx}$ is not analytically resolvable, but they did not explore the lower limit. That is, it is unclear below which level that $10^3\ln\alpha_{opx\text{-}cpx}$ becomes insensitive to Ca content in opx. Local bonding environment of Ca atoms in opx should not significantly change if Ca content is low enough, i.e. when Ca is a trace element but not a minor element in opx. Therefore, there should be a threshold concentration below which $10^3\ln\alpha_{opx\text{-}cpx}$ of $^{44}Ca/^{40}Ca$ is not sensitive to Ca concentration in opx. In order to explore opx with lower Ca content, a bigger supercell is required for the theoretical calculations. For example, at least a 240-atom supercell of opx (three times the size of the primitive cell of opx) is needed to construct the structure model with $x = 1/48$. Because the number of atoms (N) in the supercell becomes extremely large at low concentration and the computational workload is proportional to N^3, this issue could not be conveniently investigated in previous work (Feng et al., 2014).

Second, Fe is also a major element in natural opx, but it is not clear whether Fe content can affect $10^3\ln\alpha_{opx\text{-}cpx}$ of $^{44}Ca/^{40}Ca$. Kang et al. (2016) observed that Ca isotopic fractionations between opx and cpx increase with decreasing Ca content in opx, consistent with the trend from the theoretical calculations, but they are systemically smaller than the predicted equilibrium fractionation factors (Feng et al., 2014). Those discrepancies are likely due to the over-simplified model without considering the effect of Fe content in their theoretical calculations (Feng et al., 2014).

Improvements in computational capabilities in the last few years have made it possible to perform first-principles calculations for systems with more than 200 atoms. Because first-principles calculations based on the density functional theory (DFT) show comparable precision relative to the well-designed experiments (Lejaeghere et al., 2016), they have been widely used to calculate equilibrium isotope fractionation in a number of systems (Schauble et al., 2004; Méheut et al., 2009; Rustad and Yin, 2009; Schauble, 2011; Li and Liu, 2011; Kowalski and Jahn, 2011; Fujii et al., 2011, 2013, 2014; Kowalski et al., 2013; Wu et al.,

2015; Moynier and Fujii, 2017; Wang et al., 2017). Compared with Feng et al. (2014), this study focuses on the lower threshold of Ca concentration effect and the effect of Fe content in opx on $10^3\ln\alpha_{opx\text{-}cpx}$ of $^{44}Ca/^{40}Ca$. Furthermore, because Ca content in natural cpx also varies, we evaluate the effect of Ca content in cpx on $10^3\ln\alpha_{opx\text{-}cpx}$ of $^{44}Ca/^{40}Ca$ using DFT calculations. Collectively, because solid solutions are ubiquitous in natural minerals, this study provides a guideline for calculating concentration-dependent equilibrium isotope fractionation factors and understanding stable isotope data of trace elemental systematics.

2. CALCULATION METHODS

2.1. Mass-dependent equilibrium isotope fractionation factor

Mass-dependent equilibrium isotope fractionation results from the difference in vibrational frequencies due to isotopic substitution of the element of interest in two phases (Bigeleisen and Mayer, 1947; Urey, 1947). According to Richet et al. (1977), the reduced partition function ratio β_A of the element X in phase A, which represents the isotope fractionation factor between the phase A and an ideal gas of X atoms, could be expressed in the harmonic approximation as:

$$\beta_A = \frac{Q_h}{Q_l} = \prod_i^{3N} \frac{u_{ih}}{u_{il}} \frac{e^{-\frac{1}{2}u_{ih}}}{1-e^{-u_{ih}}} \frac{1-e^{-u_{il}}}{e^{-\frac{1}{2}u_{il}}} \quad (1)$$

In Eq. (1), Q is the vibrational partition function; h and l refer to the heavy and light isotope, respectively; i and N are the running indexes of vibrational frequency mode and the number of atoms in the crystal, respectively. u_{ih} or u_{il} is defined as:

$$u_{ih\,or\,il} = h\omega_{ih\,or\,il}/k_B T \quad (2)$$

where h is the Planck constant, and k_B is the Boltzmann constant; T is temperature in Kelvin, and ω_{ihoril} is the vibrational frequency of the ith mode. The equilibrium isotope fractionation between two minerals A and B can be calculated in per mil (‰) using:

$$\Delta_{A-B} = 10^3 \ln \alpha_{A-B} = 10^3 \ln \beta_A - 10^3 \ln \beta_B \quad (3)$$

2.2. First-principles calculations

The calculation details used in this study are similar to previous work (Huang et al., 2013, 2014; Feng et al., 2014; Wu et al., 2015). We performed all calculations using the software "Quantum Espresso" based on the DFT, plane wave, and pseudopotential (Giannozzi et al., 2009). The pseudopotential of Ca was generated using Vanderbilt method (Vanderbilt, 1990) with configuration $3s^23p^64s^1$ and a 1.85 Bohr cutoff radius. The pseudopotential of Mg was generated using the method of von Barth and Car (unpublished method, for a brief description of this method, see Dal Corso et al. (1993)) for all channels using a 2.5 Bohr cutoff radius and five configurations, $3s^23p^0$, $3s^13p^1$, $3s^13p^{0.5}3d^{0.5}$, $3s^13p^{0.5}$, $3s^13d^1$, with weights of 1.5, 0.6, 0.3, 0.3, 0.2, respectively. The pseudopotentials of Si and O were generated using the method of Troullier and Martins (1991) with the configuration $2s^22p^4$ and a cutoff radius of 1.45 Bohr for O and the configuration $3s^23p^43d^0$ and a cutoff radius of 1.47 Bohr for Si. The pseudopotential of Fe, Fe.pz-spn-kjpaw_psl.0.2.1.UPF, which is available in the online Quantum Espresso pseudopotential library (http://www.quantum-espresso.org/pseudopotentials/), was generated using the projector augmented-wave method (Blöchl, 1994; Kresse and Joubert, 1999) with a valence configuration of $3s^23p^64s^23d^64p^0$.

We optimized the crystal structures of Ca-doped opx and cpx with various Ca content using the method of variable cell shape molecular dynamics (Wentzcovitch, 1991) with $N_1 \times N_2 \times N_3$ k-point grid dependent on the size of unit cells (see Table S2). The plane-wave cutoff energy is 70 Ry and the residual forces converge within 10^{-4} Ry/Bohr. Their dynamical matrices were calculated on a regular q mesh dependent on the size of unit cells (Table S2) using the density-functional perturbation theory (DFPT). We used exchange correlation functional with local density approximation (LDA) (Perdew and Zunger, 1981) for calculations of Fe-free systems due to its advantages on calculating structures and thermodynamic properties of minerals (Wentzcovitch et al., 2010; Huang et al., 2013). For Fe-bearing opx, we performed LDA+U calculations because of the large on-site Coulomb interactions among Fe 3 d electrons, where the U values were non-empirically determined using linear response method (Cococcioni and de Gironcoli, 2005). After completing well structure optimizations for Fe-bearing opx, we calculated their phonon frequencies using the ab initio lattice dynamics (LD) (Alfè, 2009) method based on LDA+U.

3. RESULTS

3.1. Relaxed crystal structure

The primitive cell of Ca-free opx with 80 atoms has two non-equivalent Mg sites (M_1 and M_2). Mg atoms can be replaced by Ca atoms to form Ca-doped opx. Feng et al. (2014) found that Ca prefers the larger M_2 site, and they calculated $10^3\ln\beta$ of $^{44}Ca/^{40}Ca$ of opx with Ca content x ($Ca_xFe_yMg_{1-x-y}SiO_3$) ranging from 1/32 to 1/2. Here we expanded their compositional space, and obtained the initial structures of opx with $x = 1/48$ and $x = 1/64$ by putting one Ca atom in the M_2 site in 240-atom and 320-atom supercells, respectively.

Our calculations confirmed that Fe atoms also prefer M_2 sites in opx. Given that there are many nonequivalent configurations of opx when more than one Ca-Fe atoms are in M_2 sites, the structures with the lowest total energy were selected as the representatives and the calculated lattice parameters are listed in Table S1. There are four six-fold coordinated Mg and four eight-fold coordinated Ca sites in a primitive cell of diopside ($CaMgSi_2O_6$) with 40 atoms. A series of cpx ($CaMg_{1-x}SiO_3$) with $x = 3/8$, 5/8, 7/16, 9/16, 15/32, and 17/32 can be generated by substituting one Ca atom with one Mg atom, or vice versa, in 40-atom, 80-atom, and 160-atom structure cells of diopside. The relaxed crystal structures of opx and cpx with various

Ca content are shown in Fig. 1 with emphases on Fe—O, Mg—O and Ca—O polyhedrons, and the optimized crystal lattice parameters are listed in Table S1.

The calculation details in this study are similar to previous studies (Huang et al., 2013; Feng et al., 2014), in which the calculated cell parameters and volumes of opx

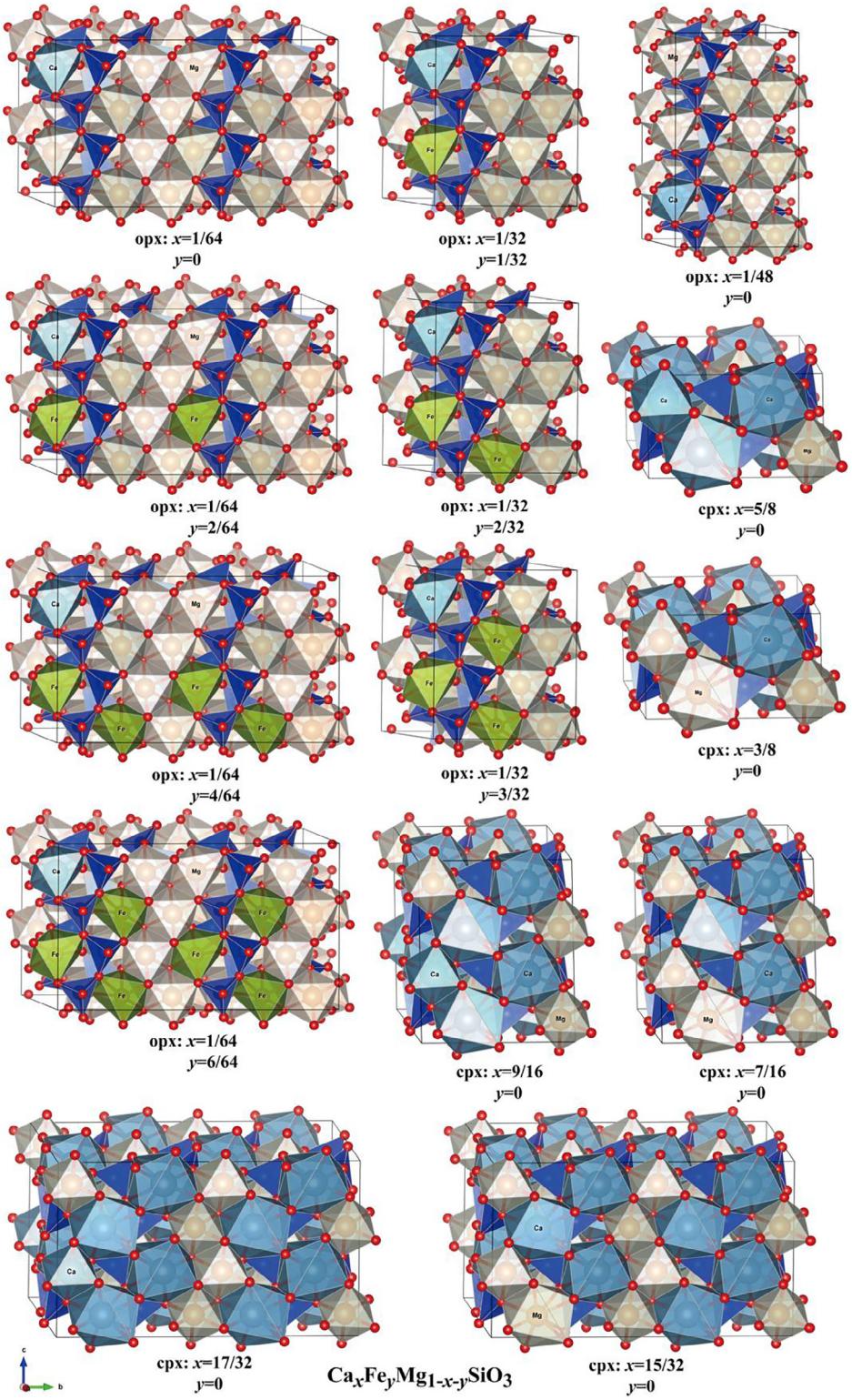

Fig. 1. Relaxed crystal structures of opx and cpx ($Ca_xFe_yMg_{1-x-y}SiO_3$) with variable x and y. Ca cations are cyan, Fe, green; Mg, brown; Si, blue; O, red. All of these crystal structures are drawn by the software "VESTA" (Momma and Izumi, 2008). (For interpretation of the references to colour in this figure legend, the reader is referred to the web version of this article.)

($Mg_2Si_2O_6$) and diopside ($CaMgSi_2O_6$) are consistent with the experimental results within 0.5% based on the LDA. Therefore, we adopted the uncertainty on $10^3\ln\beta$ and $10^3\ln\alpha$ estimated in Feng et al. (2014), which are about 5% and 7%, respectively.

3.2. Average CaO bond lengths in opx and cpx

Calculated average Ca—O bond lengths in opx and cpx are listed in Table 1 and shown in Fig. 2. The coordination number (CN) of Ca in opx depends on the accepted threshold of Ca—O bond length. Taking the maximum of Ca—O bond length in cpx as the threshold of Ca—O bond lengths in opx (Feng et al., 2014), the CN of Ca is six in opx identical to the CN of Mg in M_2 site, regardless of the different Ca and Fe contents in this study. Feng et al. (2014) found that the average Ca—O bond length decreases sharply with decreasing Ca content x in Fe-free opx from 2/16 to 1/32. Our results show that, when x drops to 1/48, the average Ca—O bond length of Fe-free opx decreases only slightly from 2.305 to 2.300 Å (Table 1), and it remains constant at 2.300 Å when x decreases further from 1/48 to 1/64 (Table 1 and Fig. 2a). That is, the average opx Ca—O bond length is sensitive to Ca content in opx only when $1/32 < x < 2/16$. Fe content can also affect the average Ca—O bond length in opx (Table 1 and Fig. 2b). When Fe content y is lower than 1/32, the effect is negligible.

Table 1
Average Ca—O bond lengths in opx and cpx.

Minerals	Ca content x	Fe content y	Average Ca—O bond length (Å)
opx ($Ca_xFe_yMg_{1-x-y}SiO_3$)	1/64	0	2.300[b]
	1/48	0	2.300[b]
	1/32	0	2.305[a]
	2/32	0	2.363[a]
	2/16	0	2.392[a]
	8/16	0	2.388[a]
	1/64	2/64	2.300[b]
	1/64	4/64	2.307[b]
	1/64	6/64	2.321[b]
	1/32	1/32	2.305[b]
	1/32	2/32	2.312[b]
	1/32	3/32	2.326[b]
cpx ($Ca_xFe_yMg_{1-x-y}SiO_3$)	3/8	0	2.459[b]
	7/16	0	2.465[b]
	15/32	0	2.469[b]
	4/8	0	2.470[a]
	17/32	0	2.467[b,*]
	9/16	0	2.462[b,*]
	5/8	0	2.453[b,*]

Clinopyroxene was calculated based on the formula of $CaMgSi_2O_6$, in which Ca and Mg are eight-fold and six-fold coordinated, respectively.

[a] Data source from Feng et al. (2014).

[b] Calculated results in this study.

[*] The structures of cpx with Ca content $x > 1/2$ (more Ca atoms in the crystal than in diopside) were formed by replacing six-fold coordinated Mg atoms in diopside with Ca atoms.

The average opx Ca—O bond length increases with increasing Fe content y when it is greater than 1/32.

Ca atoms are eight-fold coordinated and Mg atoms are six-fold in diopside ($MgCaSi_2O_6$). In cpx with Ca content $x > 4/8$, Ca atoms occupy the six-fold Mg sites. Notably, the average Ca—O bond length also varies with Ca content in Fe-free cpx and it is the longest in diopside. When x in cpx $< 4/8$, the average Ca—O bond length increases with increasing Ca content, while it decreases with increasing Ca content when $x > 4/8$ (Table 1 and Fig. 2c). Clearly, because Ca is a major element in cpx, the effect of Ca content on the average Ca—O bond length in cpx is much smaller than that in opx.

3.3. Ca isotope fractionation factors

The $10^3\ln\beta$ of $^{44}Ca/^{40}Ca$ of opx and cpx with various Ca contents are shown in Figs. 3a and 4a, and their polynomial fitting factors with temperature are reported in Table 2. $10^3\ln\alpha_{opx\text{-}diopside}$ and $10^3\ln\alpha_{cpx\text{-}diopside}$ of $^{44}Ca/^{40}Ca$ (representing the difference of $10^3\ln\beta$ between cpx and diopside) are plotted as a function of temperature in Figs. 3b and 4b, respectively. Polynomial fitting factors of $10^3\ln\alpha$ are shown in Table 3. As expected from the dependence of average Ca—O bond lengths on Ca content, $10^3\ln\beta$ of $^{44}Ca/^{40}Ca$ of opx and cpx also vary with Ca content x. In Fe-free opx, $10^3\ln\beta$ of $^{44}Ca/^{40}Ca$ with $x = 1/48$ is slightly higher than that with $x = 1/32$ by 0.04‰ at 1000 K. $10^3\ln\beta$ of $^{44}Ca/^{40}Ca$ of opx with Fe content $y = 3/32$ is lower than that of Fe-free opx with the same Ca content in opx by 0.15‰ at 1000 K. In cpx system, diopside ($MgCaSi_2O_6$) has the lowest $10^3\ln\beta$ of $^{44}Ca/^{40}Ca$, consistent with the fact that diopside has the longest average Ca—O bond length in cpx with variable Ca contents (see Fig. 4).

As a consequence, $10^3\ln\alpha$ of $^{44/}Ca/^{40}Ca$ are also affected by the Ca and Fe concentrations. For example, at 1000 K, $10^3\ln\alpha$ of $^{44}Ca/^{40}Ca$ between opx ($Mg_{47/48}Ca_{1/48}SiO_3$) and diopside is 0.64‰, slightly higher than that between $Mg_{31/32}Ca_{1/32}SiO_3$ and diopside (0.60‰). In addition, $10^3\ln\alpha$ of $^{44/}Ca/^{40}Ca$ between opx ($Mg_{(31/32-y)}Ca_{1/32}Fe_ySiO_3$) and diopside decreases from 0.60‰ to 0.46‰ with Fe content y increasing from 0 to 3/32. $10^3\ln\alpha_{cpx\text{-}diopside}$ ranges from 0.11‰ to 0.00‰ when Ca content x varies from 3/8 to 4/8 (Fig. 4).

4. DISCUSSION

4.1. Concentration effect on average CaO bond lengths in opx and cpx

Feng et al. (2014) found that the average opx Ca—O bond length increases with increasing Ca content in opx when Ca content x is lower than 2/16, while it becomes insensitive to Ca content when x is greater than 2/16. Combined with our calculations, we found that Ca concentration effect on the average opx Ca—O bond length is significant only within a certain range of Ca content with $1/48 < x < 2/16$ (Fig. 2a). When Ca is enriched in opx ($x > 2/16$), the average opx Ca—O bond length is not sensitive to Ca content, because Ca atoms play a dominant role

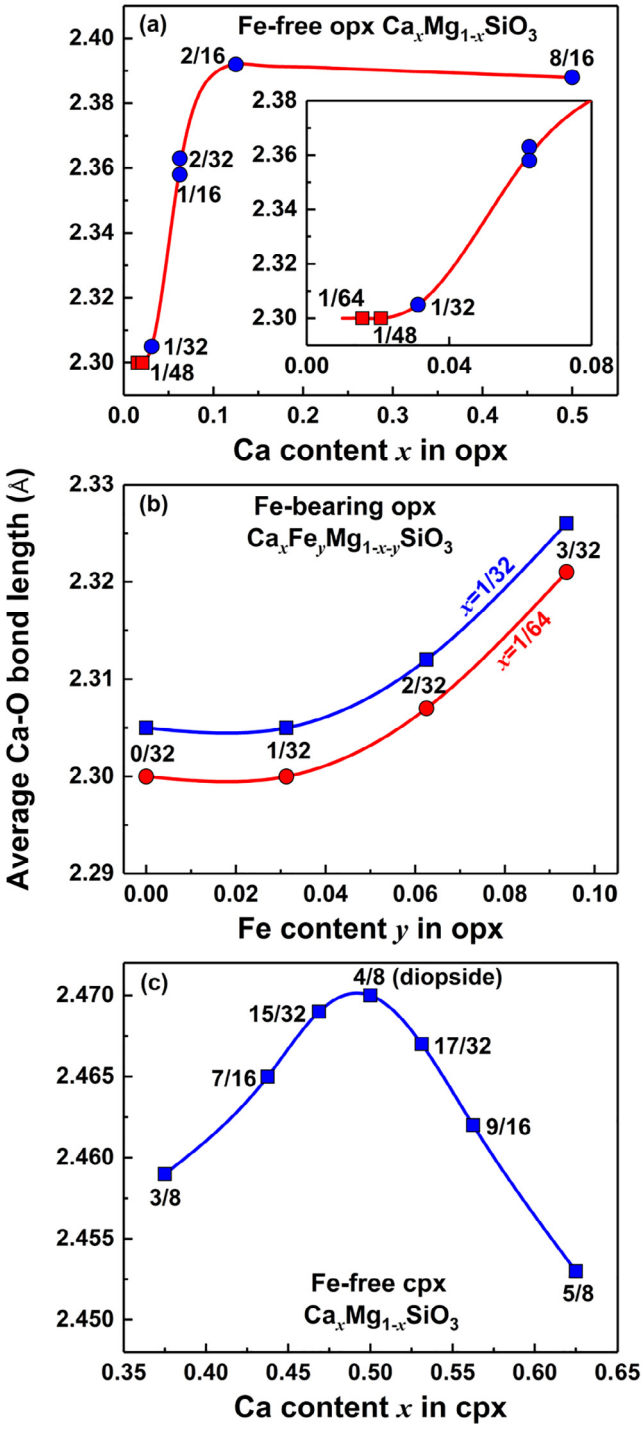

Fig. 2. Average Ca—O bond length in (a) Fe-free opx varies with Ca content x, (b) Fe-bearing opx varies with Fe content y, (c) Fe-free cpx with Ca content x.

in their local structure and Ca—O bond length tends to be a constant. With x ranging from 1/48 to 2/16, the average opx Ca—O bond length decreases dramatically with decreasing Ca content, because the Ca bonding environment is modified by its neighboring Mg and Ca atoms. Finally, when Ca content is low enough (i.e. $x < 1/48$), the average Ca—O bond length reaches a constant value and does not change with Ca content. In this case, Ca atoms are adapted to the structure controlled by Mg atoms with a much shorter Ca—O bond length than that in the structure with a high Ca content. Because the structure variation caused by the replacement of one Mg by one Ca atom is local and limited, the average Ca—O bond length should be close to a constant below a threshold

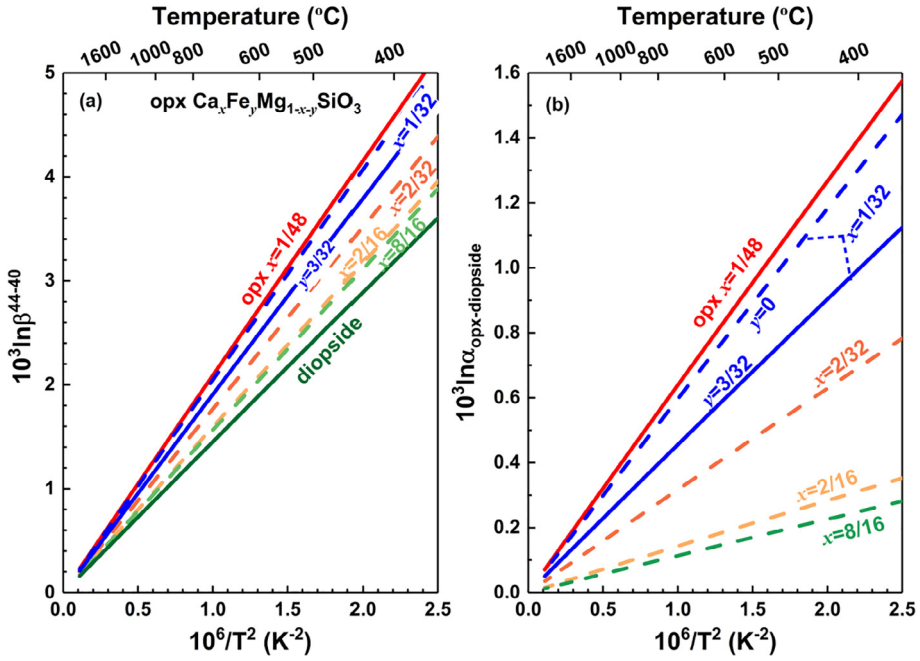

Fig. 3. (a) Calculated reduced partition function ratios of $^{44}Ca/^{40}Ca$ ($10^3 \ln \beta$) of opx ($Ca_xFe_yMg_{1-x-y}SiO_3$) with variable Ca contents and diopside ($MgCaSi_2O_6$). (b) Temperature dependence of equilibrium Ca isotope fractionation factors ($10^3 \ln \alpha$) between opx and diopside. Solid blue line represents Fe-bearing opx with $x = 1/32$ and $y = 3/32$. Other dash and solid lines are Fe-free systems. (For interpretation of the references to colour in this figure legend, the reader is referred to the web version of this article.)

Table 2
Polynomial fitting parameters of the calculated reduced partition function ratios ($10^3 \ln \beta$) of $^{44}Ca/^{40}Ca$ for opx and cpx with various Ca contents.

Minerals	Ca content x	Fe content y	a	b	c
opx ($Ca_xFe_yMg_{1-x-y}SiO_3$)	1/48†	0	2.10389	−0.01324	1.94340E−4
	1/32*	0	2.06065	−0.01265	1.88286E−4
	2/32*	0	1.77799	−0.00971	1.50828E−4
	2/16*	0	1.60256	−0.00827	1.30891E−4
	8/16*	0	1.57271	−0.0077	1.20247E−4
	1/32†	3/32	1.91804	−0.01106	1.58852E−4
cpx ($Ca_xFe_yMg_{1-x-y}SiO_3$)	3/8†	0	1.54327	−0.00761	1.26482E−4
	7/16†	0	1.49820	−0.00728	1.22401E−4
	15/32†	0	1.50261	−0.00728	1.23152E−4
	4/8*	0	1.45802	−0.00689	1.17851E−4
	17/32†	0	1.52142	−0.00759	1.26701E−4
	9/16†	0	1.53487	−0.00783	1.27937E−4
	5/8†	0	1.57114	−0.00801	1.25613E−4

$10^3 \ln \beta = az + bz^2 + cz^3$, where $z = 10^6/T^2$. T is temperature in Kelvin. Temperature range for polynomial fittings is from 673 K to 2500 K.
* Data source from Feng et al. (2014).
† Calculated results in this study.

concentration, e.g. $x = 1/48$ for opx. The varying interaction between Ca and Mg atoms with decreasing Ca content explains why there are two turning points of concentration effect on the average Ca—O bond length in opx (Fig. 2a). This phenomenon should be a common feature in solid solution systems.

The similar mechanism can be used to explain the effect of Fe content on the average Ca—O bond length in opx (Fig. 2b). Because both of $Ca^{2+}$and Fe^{2+}cations are larger than Mg^{2+}, the effect of Fe incorporation into opx on the average Ca—O bond length should be similar to that of Ca. Similar to Ca, increasing Fe content y cannot significantly increase the average Ca—O bond length when Fe content in opx is low (i.e. $y < 1/32$). As mentioned above, the average Ca—O bond length sharply increases with Ca content x when $x > 1/32$ (Fig. 2a), and increasing Fe content also increases the average opx Ca—O bond length (Fig. 2b). However, the average Ca—O bond length is more sensitive to the variation of Ca content than Fe content since the radius of $Ca^{2+}$is much larger than Fe^{2+}. For

Table 3
Polynomial fitting parameters of equilibrium isotope fractionation factors ($10^3 \ln \alpha$) of $^{44}Ca/^{40}Ca$ between minerals (including opx with different Ca and Fe contents and cpx with variable Ca contents) and diopside.

Minerals	Ca content x	Fe content y	a	b	c
opx ($Ca_xFe_yMg_{1-x-y}SiO_3$)	1/48[†]	0	0.64587	−0.00635	7.6489E−05
	1/32[*]	0	0.60263	−0.00576	7.0435E−05
	2/32[*]	0	0.31997	−0.00282	3.2977E−05
	2/16[*]	0	0.14454	−0.00138	1.3040E−05
	8/16[*]	0	0.11469	−0.00081	2.3960E−06
	1/32[†]	3/32	0.46002	−0.00417	4.1001E−05
cpx ($Ca_xFe_yMg_{1-x-y}SiO_3$)	3/8[†]	0	0.08525	−0.00072	8.6310E−06
	7/16[†]	0	0.04018	−0.00039	4.5500E−06
	15/32[†]	0	0.04459	−0.00039	5.3010E−06
	17/32[†]	0	0.06340	−0.00070	8.8500E−06
	9/16[†]	0	0.07685	−0.00094	1.0086E−05
	5/8[†]	0	0.11312	−0.00112	7.7620E−06

$10^3 \ln \alpha = az + bz^2 + cz^3$, where $z = 10^6/T^2$. T is temperature in Kelvin. Temperature range for polynomial fittings is from 673 K to 2500 K.
[*] Data source from Feng et al. (2014).
[†] Calculated results in this study.

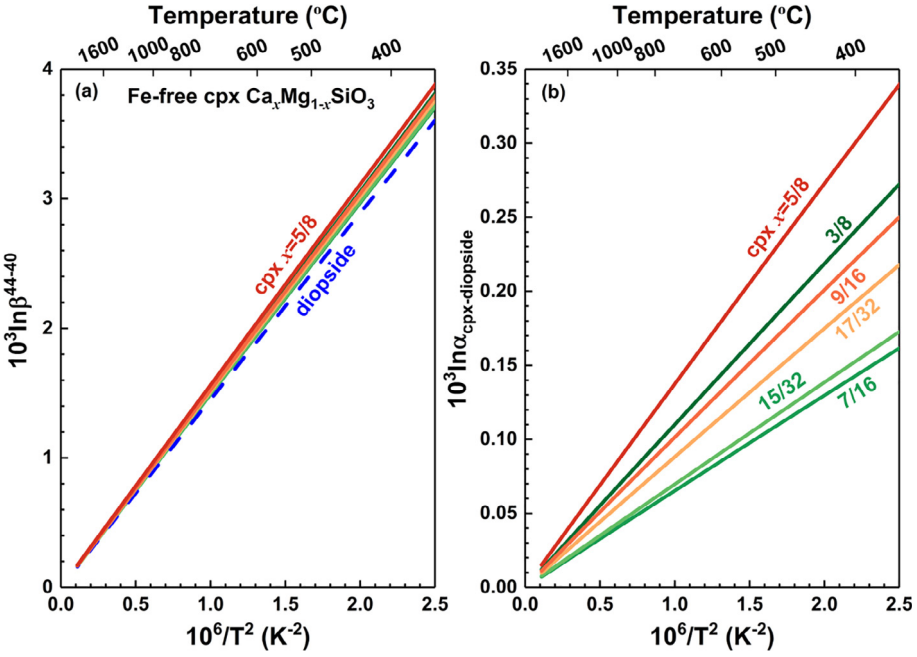

Fig. 4. (a) Calculated reduced partition function ratios of $^{44}Ca/^{40}Ca$ ($10^3 \ln \beta$) of Fe-free cpx with variable Ca contents. (b) Temperature dependence of equilibrium Ca isotope fractionation factors ($10^3 \ln \alpha_{cpx-diopside}$) between Fe-free cpx and diopside.

example, for opx with $x = 1/32$, the average Ca—O bond length slightly increases from 2.305 Å to 2.312 Å when y in opx increases from 1/32 to 2/32. For comparison, in Fe-free opx, it increases from 2.305 Å to 2.363 Å when x increases from 1/32 to 2/32. Fe content (y) in natural opx is ~0.1 (such as in mantle peridotites), which can increase the average Ca—O bond length by 0.007 Å compared to Fe-free opx (Table 1 and Fig. 2b).

Ca content can also modify the average Ca—O bond length in Fe-free cpx (Table 1 and Fig. 2c). Diopside has the largest average Ca—O bond length among all pyroxene minerals calculated in this study. The average Ca—O bond length in cpx increases with increasing Ca content when $x < 1/2$, while it decreases with increasing Ca content when $x > 1/2$. In the 40-atom cell of diopside ($MgCaSi_2O_6$), the four sites of six-fold coordinated Mg sites are not equivalent to the four sites of eight-fold coordinated Ca sites. When x is lower than 1/2, Mg atoms occupy Ca sites in cpx and all Ca atoms are eight-fold coordinated. In cpx with $x > 1/2$, Ca atoms begin to occupy the sixf-old coordinated Mg sites, so that these "six-fold coordinated" Ca atoms have shorter Ca—O bond lengths, causing the negative dependence of average Ca—O bond length on Ca content in cpx. Therefore, the dependence of average Ca—O

bond length in cpx on Ca content is similar to that in opx. In general, as a major element in cpx, the effect of Ca content on average Ca—O bond length is small. Ca content (x) in natural occurring cpx ranges from 0.44 to 0.5, causing a relative variation of ~0.2% in their average Ca—O bond length. Because the effect of Fe content on the average Ca—O bond length in opx is less significant than Ca content, incorporating Fe into cpx is not expected to significantly influence the average Ca—O bond length in cpx.

4.2. Concentration effect on equilibrium Ca isotope fractionation

Combining our results with published theoretical calculations (Feng et al., 2014), we found that $10^3\ln\alpha_{\text{opx-diopside}}$ of $^{44}Ca/^{40}Ca$ are linearly correlated with average Ca—O bond lengths in opx (Fig. 5a), including both Fe-free and Fe-bearing opx. Equilibrium isotope fractionations are controlled by relevant bond strengths, which are usually affected by bond lengths and coordinate numbers (CN). Since Ca atoms in opx occupy Mg sites with a CN of six, the average Ca—O bond length of opx dominantly determines $10^3\ln\alpha_{\text{opx-diopside}}$. In general, shorter chemical bonds have stronger bond strengths and higher vibrational frequencies, which are enriched in heavier isotopes relative to longer chemical bonds (Urey, 1947; Schauble et al., 2004; Hill and Schauble, 2008; Young et al., 2009). Therefore, the dependence of average Ca—O bond lengths on Ca content in opx determines the relationship between $10^3\ln\alpha_{\text{opx-diopside}}$ of $^{44}Ca/^{40}Ca$ and Ca content in opx (Fig. 5b). Although we did not calculate $10^3\ln\beta$ of $^{44}Ca/^{40}Ca$ of opx with $x = 1/64$ using a 320-atom supercell due to the limitation of our computation capabilities, we can predict that the $10^3\ln\beta$ of $^{44}Ca/^{40}Ca$ of opx with $x = 1/64$ is similar to that of opx with $x = 1/48$ because they have the identical average Ca—O bond length.

In Fig. 5b, $103\ln\alpha_{\text{opx-diopside}}$ of $^{44}Ca/^{40}Ca$ is plotted as a function of Ca content in opx at different temperatures. When Ca content x in opx is lower than 1/48, $10^3\ln\alpha_{\text{opx-diopside}}$ of $^{44}Ca/^{40}Ca$ does not vary with Ca content; in contrast, Ca content of opx shows a strong impact on $10^3\ln\alpha_{\text{opx-diopside}}$ of $^{44}Ca/^{40}Ca$ when x ranges from 1/32 to 2/16. Notably, $10^3\ln\beta$ of opx with $x = 1/32$ is already very close to that of opx with $x = 1/48$ (Fig. 3a), suggesting that opx with $x = 1/48$ can be selected as a good representative to calculate equilibrium Ca isotope fractionation for opx with extremely low Ca content (<3 mol%). The fitting equation $10^3\ln\alpha_{opx-diopside} = \frac{0.53\times10^6}{T^2}\frac{1}{1+e^{(x-0.074)*80}} + \frac{0.114\times10^6}{T^2}$, in which x ranges from 0 to 0.5 and T is greater than 700 K, can be used to illustrate the dependences of $10^3\ln\alpha_{opx-diopside}$ on Ca content (x) in opx and temperature T. The incorporation of Fe into opx crystal structure increases the average Ca—O bond length in opx (Fig. 2b) when Fe content y is greater than 1/32, leading to a decrease of $10^3\ln\alpha_{\text{opx-diopside}}$ of $^{44}Ca/^{40}Ca$ compared to $10^3\ln\alpha_{\text{Fe-free opx-diopside}}$.

The difference of $10^3\ln\beta$ of $^{44}Ca/^{40}Ca$ between cpx and diopside (expressed as $10^3\ln\alpha_{\text{cpx-diopside}}$), is linearly correlated with the average Ca—O bond length in cpx (Fig. 6a), indicating that the effect of Ca content in cpx on $10^3\ln\alpha_{\text{cpx-diopside}}$ is also related to the controlling of average Ca—O bond length in cpx by Ca content (Fig. 6b). However, the variation in Ca concentration of cpx shows a negligible effect at high temperature. For example, $10^3\ln\alpha_{\text{cpx-diopside}}$ is only ~0.05‰ at 1200 K when Ca content x ranges from 0.45 to 0.5.

4.3. Implications for Ca isotope fractionation between opx and cpx

Understanding of inter-mineral Ca isotope fractionation mechanism is the base for applying Ca isotopes to investigate geochemical and cosmochemical processes. Opx and cpx are two major host minerals of Ca in the upper mantle, and their Ca isotopic variations are critical in determining the Ca isotopic composition and evolution of the upper mantle. Huang et al. (2010) reported that Kilbourne Hole peridotite has cpx $\delta^{44/40}Ca$ of 0.98 ± 0.04‰ (2se) and opx $\delta^{44/40}Ca$ of 1.73 ± 0.09‰, while San Carlos peridotite has cpx $\delta^{44/40}Ca$ of 1.04 ± 0.04‰ and opx $\delta^{44/40}Ca$ of 1.40 ± 0.07‰, demonstrating a large variation of $\Delta^{44/40}Ca_{\text{opx-cpx}}$ from 0.36‰ to 0.75‰. $\delta^{44/40}Ca$ of cpx from mantle xenoliths reported by Kang et al. (2016) varies from

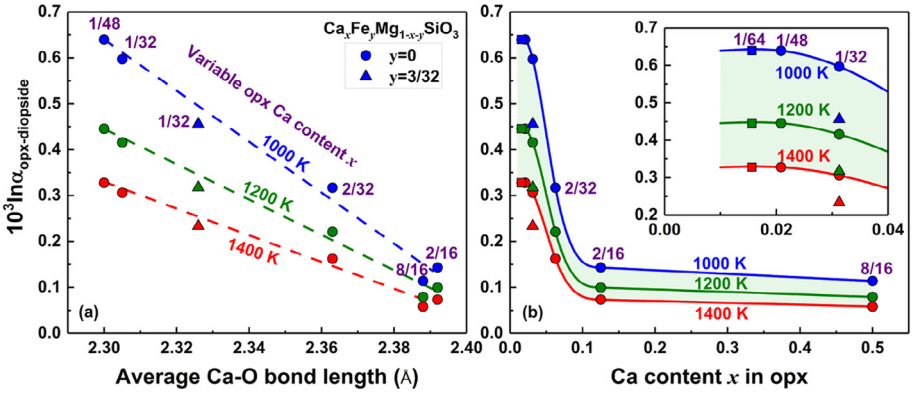

Fig. 5. Correlations between (a) $10^3\ln\alpha_{opx-diopside}$ and average Ca—O bond length in opx with variable Ca contents, (b) $10^3\ln\alpha_{opx-diopside}$ and Ca content in opx. Circles and triangles represent Fe-free and Fe-bearing opx, respectively. $10^3\ln\alpha_{opx-diopside}$ can be expressed as a function of Ca content x and temperature (T): $10^3\ln\alpha_{opx-diopside} = \frac{0.53\times10^6}{T^2}\frac{1}{1+e^{(x-0.074)*80}} + \frac{0.114\times10^6}{T^2}$, in which x ranges from 0 to 0.5 and T is greater than 700 K.

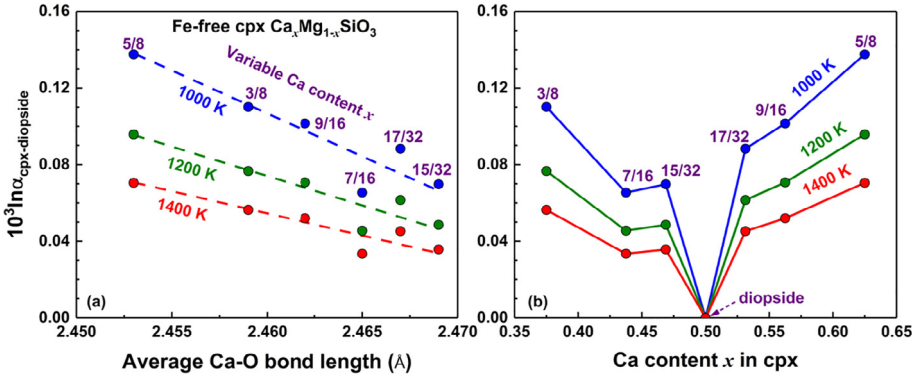

Fig. 6. Correlations between (a) $10^3 \ln \alpha_{cpx-diopside}$ and average Ca—O bond length in Fe-free cpx with variable Ca contents, (b) $10^3 \ln \alpha_{cpx-diopside}$ and Ca content in Fe-free cpx.

$0.71 \pm 0.06‰$ to $1.03 \pm 0.12‰$ and the co-existing opx from $0.95 \pm 0.05‰$ to $1.82 \pm 0.01‰$, leading to a large variation in $\Delta^{44/40}Ca_{opx\text{-}cpx}$ ranging from $-0.01‰$ to $1.11‰$, which is negatively correlated with Ca content in opx. More recently, $\Delta^{44/40}Ca_{opx\text{-}cpx}$ from Yangyuan peridotites reported by Zhao et al. (2017) shows a large variation ranging from $-0.49‰$ to $0.31‰$. The Ca concentration effect was originally proposed to account for these observations (Feng et al., 2014; Kang et al., 2016), assuming that variations of Ca content in opx also strongly influences $10^3 ln\alpha_{opx\text{-}cpx}$ when Ca content $x < 1/32$. However, according to our calculated results, $10^3 ln\alpha_{opx\text{-}cpx}$ does not significantly vary with Ca content in opx when $x < 1/32$. Instead, it maintains a constant when $x < 1/48$. Although variations of Fe content in opx could modify $10^3 ln\alpha_{opx\text{-}cpx}$, the existence of Fe in opx will cause a uniform decrease in $10^3 ln\alpha_{opx\text{-}cpx}$ at different Ca contents because Fe contents in natural occurring opx are ~10 mol% (Fig. 7a). With Ca content of opx fixed, compared to the Fe-free opx, $10^3 ln\alpha_{opx\text{-}cpx}$ with Fe content y of 3/32 in opx reduces by 0.14‰ at 1000 K and 0.07‰ at 1400 K (Fig. 7a).

Our calculations suggest that $10^3 ln\alpha_{opx\text{-}cpx}$ is not affected by Ca content in opx when Ca content of opx is comparable to that in natural opx samples. Rather, $10^3 ln\alpha_{opx\text{-}cpx}$ is dominantly controlled by temperature (Fig. 7a). At a fixed Fe content in opx ($y = 3/32$), $10^3 ln\alpha_{opx\text{-}cpx}$ decreases from 0.50‰ to 0.26‰ when temperature increases from 1000 K to 1400 K. Although a large temperature variation (>200 K) may explain the considerable difference within uncertainty in $\Delta^{44/40}Ca_{opx\text{-}cpx}$ (0.36‰ vs. 0.75‰) in San Carlos and Kilbourne Hole mantle peridotites if both reached isotope equilibrium, the large variations of $\Delta^{44/40}Ca_{opx\text{-}cpx}$ in Hannuoba peridotites ($-0.01‰$ to $1.11‰$) and Yangyuan peridotites ($-0.49‰$ to $0.31‰$) cannot result from equilibrium fractionation at variable temperatures. Moreover, the variation in Ca content of cpx ($0.4 < x < 0.5$) shows a negligible effect on $10^3 ln\alpha_{opx\text{-}cpx}$ (Fig. 7b), and it cannot account for the large variations of $\Delta^{44/40}Ca_{opx\text{-}cpx}$. Therefore, our results suggest that $\Delta^{44/40}Ca_{opx\text{-}cpx}$ from natural peridotites deviating from the equilibrium range (0.26–0.50‰) may indicate Ca isotope disequilibrium. For such case, these abnormal $\Delta^{44/40}Ca_{opx\text{-}cpx}$ can be used to study mantle

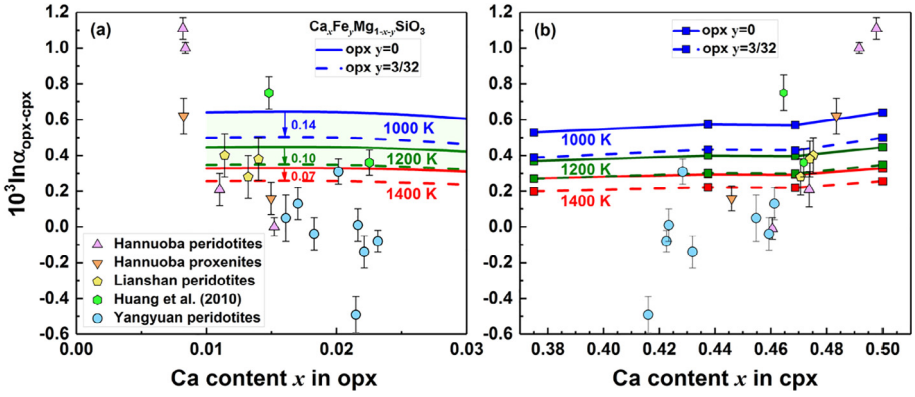

Fig. 7. Equilibrium Ca isotopes fractionation factors ($10^3 \ln \alpha_{opx-cpx}$) between Fe-free (solid curves) and Fe-bearing (dash curves) opx with variable Ca contents and cpx. Squares are calculated results fitted by solid curves. (a) Relationship between $10^3 \ln \alpha_{opx-cpx}$ and Ca content in opx. (b) Relationship between $10^3 \ln \alpha_{opx-cpx}$ and Ca content in cpx. Dash curves are obtained from the difference between opx with $y = 0$ and opx with $y = 3/32$ when $x = 1/32$. Data sources of natural samples: hexagons, Huang et al. (2010); regular pentagons, triangles and inverted triangles, Kang et al. (2016); circles, Zhao et al. (2017).

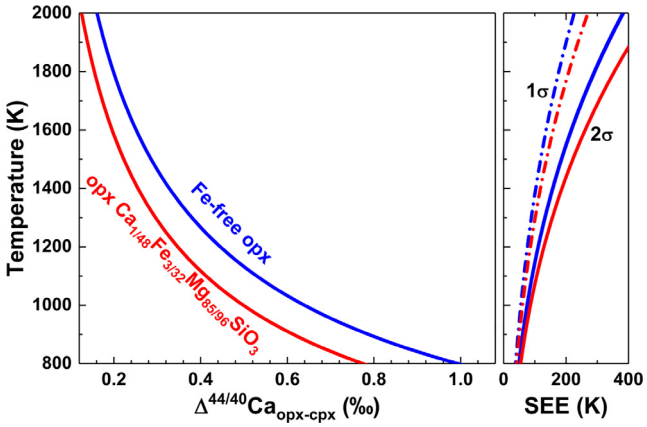

Fig. 8. Correlation between temperature and $\Delta^{44/40}Ca_{opx-cpx}$ as a potential Ca isotope thermometer. SEE is standard error of the estimation. Blue and red curves represent opx with $y = 0$ and $y = 3/32$. (For interpretation of the references to colour in this figure legend, the reader is referred to the web version of this article.)

processes such as melt-rock interaction, metasomatism, and kinetic effect (Young et al., 2009; Zhao et al., 2017).

4.4. Opx-cpx Ca isotope thermometer

Feng et al. (2014) found that Ca content in opx has significant effect on $10^3\ln\alpha_{opx\text{-}cpx}$ when x in opx ($Ca_xFe_yMg_{1-x-y}SiO_3$) ranges from 2/16 to 1/32, while our results further suggest that $10^3\ln\alpha_{opx\text{-}cpx}$ is not controlled by Ca content in opx but only depends on temperature when $x < 1/48$. Therefore, equilibrium Ca isotopes fractionation between cpx and naturally occurring opx usually with $x < 1/48$ is equal to $10^3\ln\alpha$ between cpx and opx with $x = 1/48$ after the correction of Fe effect (Fig. 7a). Because $10^3\ln\alpha_{opx\text{-}cpx}$ is sensitive to temperature, the relationship between $10^3\ln\alpha_{opx\text{-}cpx}$ and temperature could be used as a two pyroxene Ca isotope thermometer (Fig. 8). For example, the estimated $10^3\ln\alpha_{opx\text{-}cpx}$ ranging from 0.37‰ to 0.49‰ corresponds to temperature decreasing from 1200 K to 1000 K. Standard error of the estimation (SEE) of temperature can be obtained based on the current analytical precision (0.05‰, 2se) (e.g. Simon and DePaolo, 2010; Lehn et al., 2013; Kang et al., 2016; Huang and Jacobsen, 2017; Zhao et al., 2017) and the uncertainty of $10^3\ln\alpha_{opx\text{-}cpx}$. For example, the 1σ standard error at 1200 K is about 70 K using our two pyroxene Ca isotope thermometer, which is comparable to that of the elemental geothermometer (e.g. Putirka, 2008, 2016). Therefore, the two pyroxene Ca isotope thermometer may provide an independent useful tool to determine their equilibrium temperatures.

5. CONCLUSIONS

We examine the effect of Ca and Fe contents in opx ($Ca_xFe_yMg_{1-x-y}SiO_3$) on $10^3\ln\alpha_{opx\text{-}cpx}$ of $^{44}Ca/^{40}Ca$ using first-principles calculations. The results show that the average Ca—O bond length in Fe-free opx decreases slightly from 2.305 to 2.30 Å when x drops from 1/32 to 1/48, and remains constant when x changes from 1/48 to 1/64, suggesting that Ca concentration effect on the average Ca—O bond length is significant only within a certain range of Ca content. When y in opx is lower than 1/32, the Fe effect on the average Ca—O bond length is negligible, while the average Ca—O bond length increases with increasing Fe content when y is greater than 1/32. $10^3\ln\alpha_{opx\text{-}cpx}$ of $^{44}Ca/^{40}Ca$ are linearly correlated with opx average Ca—O bond lengths. Consequently, $10^3\ln\alpha_{opx\text{-}cpx}$ of $^{44}Ca/^{40}Ca$ remains constant with decreasing Ca content in opx when $x < 1/48$. Although variations of Fe content in opx could modify $10^3\ln\alpha_{opx\text{-}cpx}$, the existence of Fe in opx causes a uniformly small decrease in $10^3\ln\alpha_{opx\text{-}cpx}$ at different Ca contents because Fe contents in opx from natural samples are ~10 mol%. Moreover, the variation in Ca concentration of cpx shows negligible effect on $10^3\ln\alpha_{opx\text{-}cpx}$ because Ca is a major element in cpx.

This study provides a guideline for the applications of Ca isotopes into high temperature geochemical and cosmochemical processes. Our results suggest that $10^3\ln\alpha_{opx\text{-}cpx}$ is mainly controlled by temperature, but not affected by Ca content in opx in natural peridotites because of their low Ca contents. With temperature increasing from 1000 K to 1400 K, $10^3\ln\alpha_{opx\text{-}cpx}$ decreases from 0.50‰ to 0.26‰. Therefore, the large variation of $\Delta^{44/40}Ca_{opx\text{-}cpx}$ in peridotites and pyroxenites in the literature (−0.49‰ to 1.11‰) cannot result from equilibrium isotope fractionation. Other processes must be involved, such as mantle metasomatism and chemical diffusion. Finally, because equilibrium Ca isotope fractionation between natural opx and cpx is sensitive to temperature, it can be used as a two-pyroxene Ca isotope thermometer, with the estimated temperature precision comparable to that of elemental geothermometer.

ACKNOWLEDGMENTS

This work is financially supported by the Natural Science Foundation of China (41473011, 41325011, 41090370), the 111 project, the Fundamental Research Funds for the Central Universities (WK2080000078), and Special Program for Applied Research on Super Computation of the NSFC-Guangdong Joint Fund. Shichun Huang acknowledges support from NSF grant EAR-1524387. The computations were conducted partly in Supercomputing Center of the University of Science and Technology of China. We are grateful

to the constructive comments from three anonymous reviewers and editorial handling by Frédéric Moynier.

APPENDIX A. SUPPLEMENTARY MATERIAL

Supplementary data associated with this article can be found, in the online version, at https://doi.org/10.1016/j.gca.2017.09.022.

REFERENCES

Alfè D. (2009) PHON: a program to calculate phonons using the small displacement method. *Comput. Phys. Commun.* **180**, 2622–2633.

Amsellem E., Moynier F., Pringle E. A., Bouvier A., Chen H. and Day J. M. D. (2017) Testing the chondrule-rich accretion model for planetary embryos using calcium isotopes. *Earth Planet. Sci. Lett.* **469**, 75–83.

An Y., Huang J.-X., Griffin W. L., Liu C. and Huang F. (2017) Isotopic composition of Mg and Fe in garnet peridotites from the Kaapvaal and Siberian cratons. *Geochim. Cosmochim. Acta* **200**, 167–185.

Anderson J. L., Barth A. P., Wooden J. L. and Mazdab F. (2008) Thermometers and thermobarometers in granitic systems. *Rev. Mineral. Geochem.* **69**, 121–142.

Beattie P. (1993) Olivine-melt and orthopyroxene-melt equilibria. *Contrib. Mineral. Petrol.* **115**, 103–111.

Benisek A., Kroll H. and Cemič L. (2004) New developments in two-feldspar thermometry. *Am. Mineral.* **89**, 1496–1504.

Bigeleisen J. and Mayer M. G. (1947) Calculation of equilibrium constants for isotopic exchange reactions. *J. Chem. Phys.* **15**, 261.

Blöchl P. E. (1994) Projector augmented-wave method. *Phys. Rev. B* **50**, 17953–17979.

Brey G. P. and Köhler T. (1990) Geothermobarometry in four-phase Lherzolites II. New thermobarometers, and practical assessment of existing thermobarometers. *J. Petrol.* **31**, 1353–1378.

Brown W. L. and Parsons I. (1981) Towards a more practical two-feldspar geothermometer. *Contrib. Mineral. Petrol.* **76**, 369–377.

Cococcioni M. and de Gironcoli S. (2005) Linear response approach to the calculation of the effective interaction parameters in the LDA+U method. *Phys. Rev. B* **71**, 35105.

Dal Corso A., Baroni S., Resta R. and de Gironcoli S. (1993) Ab initio calculation of phonon dispersions in II–VI semiconductors. *Phys. Rev. B* **47**, 3588.

DePaolo D. J. (2004) Calcium isotopic variations produced by biological, kinetic, radiogenic and nucleosynthetic processes. *Rev. Mineral. Geochem.* **55**, 255–288.

Feng C., Qin T., Huang S., Wu Z. and Huang F. (2014) First-principles investigations of equilibrium calcium isotope fractionation between clinopyroxene and Ca-doped orthopyroxene. *Geochim. Cosmochim. Acta* **143**, 132–142.

Fujii T., Moynier F., Abe M., Nemoto K. and Albarède F. (2013) Copper isotope fractionation between aqueous compounds relevant to low temperature geochemistry and biology. *Geochim. Cosmochim. Acta* **110**, 29–44.

Fujii T., Moynier F., Blichert-Toft J. and Albarède F. (2014) Density functional theory estimation of isotope fractionation of Fe, Ni, Cu, and Zn among species relevant to geochemical and biological environments. *Geochim. Cosmochim. Acta* **140**, 553–576.

Fujii T., Moynier F., Pons M.-L. and Albarède F. (2011) The origin of Zn isotope fractionation in sulfides. *Geochim. Cosmochim. Acta* **75**, 7632–7643.

Giannozzi P., Baroni S., Bonini N., Calandra M., Car R., Cavazzoni C., Ceresoli D., Chiarotti G. L., Cococcioni M., Dabo I., Dal Corso A., de Gironcoli S., Fabris S., Fratesi G., Gebauer R., Gerstmann U., Gougoussis C., Kokalj A., Lazzeri M., Martin-Samos L., Marzari N., Mauri F., Mazzarello R., Paolini S., Pasquarello A., Paulatto L., Sbraccia C., Scandolo S., Sclauzero G., Seitsonen A. P., Smogunov A., Umari P. and Wentzcovitch R. M. (2009) QUANTUM ESPRESSO: a modular and open-source software project for quantum simulations of materials. *J. Phys. Condens. Matter* **21**, 395502.

Halicz L., Galy A., Belshaw N. S. and O'Nions R. K. (1999) High-precision measurement of calcium isotopes in carbonates and related materials by multiple collector inductively coupled plasma mass spectrometry (MC-ICP-MS). *J. Anal. At. Spectrom.* **14**, 1835–1838.

Hill E., Wood B. J. and Blundy J. D. (2000) The effect of Ca-Tschermaks component on trace element partitioning between clinopyroxene and silicate melt. *Lithos* **53**, 203–215.

Hill P. S. and Schauble E. A. (2008) Modeling the effects of bond environment on equilibrium iron isotope fractionation in ferric aquo-chloro complexes. *Geochim. Cosmochim. Acta* **72**, 1939–1958.

Holmden C. (2009) Ca isotope study of Ordovician dolomite, limestone, and anhydrite in the Williston Basin: implications for subsurface dolomitization and local Ca cycling. *Chem. Geol.* **268**, 180–188.

Huang F., Chen L., Wu Z. and Wang W. (2013) First-principles calculations of equilibrium Mg isotope fractionations between garnet, clinopyroxene, orthopyroxene, and olivine: Implications for Mg isotope thermometry. *Earth Planet. Sci. Lett.* **367**, 61–70.

Huang F., Wu Z., Huang S. and Wu F. (2014) First-principles calculations of equilibrium silicon isotope fractionation among mantle minerals. *Geochim. Cosmochim. Acta* **140**, 509–520.

Huang S., Farkaš J. and Jacobsen S. B. (2010) Calcium isotopic fractionation between clinopyroxene and orthopyroxene from mantle peridotites. *Earth Planet. Sci. Lett.* **292**, 337–344.

Huang S., Farkaš J. and Jacobsen S. B. (2011) Stable calcium isotopic compositions of Hawaiian shield lavas: evidence for recycling of ancient marine carbonates into the mantle. *Geochim. Cosmochim. Acta* **75**, 4987–4997.

Huang S., Farkaš J., Yu G., Petaev M. I. and Jacobsen S. B. (2012) Calcium isotopic ratios and rare earth element abundances in refractory inclusions from the Allende CV3 chondrite. *Geochim. Cosmochim. Acta* **77**, 252–265.

Huang S. and Jacobsen S. B. (2017) Calcium isotopic compositions of chondrites. *Geochim. Cosmochim. Acta* **201**, 364–376.

Jacobson A. D. and Holmden C. (2008) Δ^{44}Ca evolution in a carbonate aquifer and its bearing on the equilibrium isotope fractionation factor for calcite. *Earth Planet. Sci. Lett.* **270**, 349–353.

Kang J., Zhu H., Liu Y.-F., Liu F., Wu F., Hao Y.-T., Zhi X.-C., Zhang Z.-F. and Huang F. (2016) Calcium isotopic composition of mantle xenoliths and minerals from Eastern China. *Geochim. Cosmochim. Acta* **174**, 335–344.

Kasemann S. A., Hawkesworth C. J., Prave A. R., Fallick A. E. and Pearson P. N. (2005) Boron and calcium isotope composition in Neoproterozoic carbonate rocks from Namibia: evidence for extreme environmental change. *Earth Planet. Sci. Lett.* **231**, 73–86.

Kowalski P. M. and Jahn S. (2011) Prediction of equilibrium Li isotope fractionation between minerals and aqueous solutions

at high P and T: an efficient ab initio approach. *Geochim. Cosmochim. Acta* **75**, 6112–6123.

Kowalski P. M., Wunder B. and Jahn S. (2013) Ab initio prediction of equilibrium boron isotope fractionation between minerals and aqueous fluids at high P and T. *Geochim. Cosmochim. Acta* **101**, 285–301.

Kresse G. and Joubert D. (1999) From ultrasoft pseudopotentials to the projector augmented-wave method. *Phys. Rev. B* **59**, 1758–1775.

Lehn G. O., Jacobson A. D. and Holmden C. (2013) Precise analysis of Ca isotope ratios (δ44/40Ca) using an optimized ^{43}Ca–^{42}Ca double-spike MC-TIMS method. *Int. J. Mass Spectrom.* **351**, 69–75.

Lejaeghere K., Bihlmayer G., Bjorkman T., Blaha P., Blugel S., Blum V., Caliste D., Castelli I. E., Clark S. J., Dal Corso A., de Gironcoli S., Deutsch T., Dewhurst J. K., Di Marco I., Draxl C., Du ak M., Eriksson O., Flores-Livas J. A., Garrity K. F., Genovese L., Giannozzi P., Giantomassi M., Goedecker S., Gonze X., Granas O., Gross E. K. U., Gulans A., Gygi F., Hamann D. R., Hasnip P. J., Holzwarth N. A. W., Iu an D., Jochym D. B., Jollet F., Jones D., Kresse G., Koepernik K., Kucukbenli E., Kvashnin Y. O., Locht I. L. M., Lubeck S., Marsman M., Marzari N., Nitzsche U., Nordstrom L., Ozaki T., Paulatto L., Pickard C. J., Poelmans W., Probert M. I. J., Refson K., Richter M., Rignanese G.-M., Saha S., Scheffler M., Schlipf M., Schwarz K., Sharma S., Tavazza F., Thunstrom P., Tkatchenko A., Torrent M., Vanderbilt D., van Setten M. J., Van Speybroeck V., Wills J. M., Yates J. R., Zhang G.-X. and Cottenier S. (2016) Reproducibility in density functional theory calculations of solids. *Science* 351, aad3000–aad3000.

Li X. and Liu Y. (2011) Equilibrium Se isotope fractionation parameters: A first-principles study. *Earth Planet. Sci. Lett.* **304**, 113–120.

Lundstrom C., Shaw H., Ryerson F., Williams Q. and Gill J. (1998) Crystal chemical control of clinopyroxene-melt partitioning in the Di-Ab-An system: implications for elemental fractionations in the depleted mantle. *Geochim. Cosmochim. Acta* **62**, 2849–2862.

Méheut M., Lazzeri M., Balan E. and Mauri F. (2009) Structural control over equilibrium silicon and oxygen isotopic fractionation: a first-principles density-functional theory study. *Chem. Geol.* **258**, 28–37.

Momma K. and Izumi F. (2008) VESTA: a three-dimensional visualization system for electronic and structural analysis. *J. Appl. Crystallogr.* **41**, 653–658.

Moynier F. and Fujii T. (2017) Calcium isotope fractionation between aqueous compounds relevant to low-temperature geochemistry, biology and medicine. *Sci. Rep.* **7**, 44255.

Perdew J. P. and Zunger A. (1981) Self-interaction correction to density-functional approximations for many-electron systems. *Phys. Rev. B* **23**, 5048–5079.

Putirka K. (2016) Amphibole thermometers and barometers for igneous systems and some implications for eruption mechanisms of felsic magmas at arc volcanoes. *Am. Mineral.* **101**, 841–858.

Putirka K. D. (2008) Thermometers and barometers for volcanic systems. *Rev. Mineral. Geochem.* **69**, 61–120.

Richet P., Bottinga Y. and Javoy M. (1977) A review of hydrogen, carbon, nitrogen, oxygen, sulphur, and chlorine stable isotope fractionation among gaseous molecules. *Annu. Rev. Earth Planet. Sci.* **5**, 65–110.

Rustad J. R. and Yin Q.-Z. (2009) Iron isotope fractionation in the Earth's lower mantle. *Nat. Geosci.* **2**, 514–518.

Schauble E. A. (2011) First-principles estimates of equilibrium magnesium isotope fractionation in silicate, oxide, carbonate and hexaaquamagnesium(2+) crystals. *Geochim. Cosmochim. Acta* **75**, 844–869.

Schauble E., Rossman G. R. and Taylor H. P. (2004) Theoretical estimates of equilibrium chromium-isotope fractionations. *Chem. Geol.* **205**, 99–114.

Simon J. I. and DePaolo D. J. (2010) Stable calcium isotopic composition of meteorites and rocky planets. *Earth Planet. Sci. Lett.* **289**, 457–466.

Simon J. I., DePaolo D. J. and Moynier F. (2009) Calcium isotope composition of meteorites, earth, and mars. *Astrophys. J.* **702**, 707–715.

Steuber T. and Buhl D. (2006) Calcium-isotope fractionation in selected modern and ancient marine carbonates. *Geochim. Cosmochim. Acta* **70**, 5507–5521.

Troullier N. and Martins J. L. (1991) Efficient pseudopotentials for plane-wave calculations. II. Operators for fast iterative diagonalization. *Phys. Rev. B* **43**, 8861–8869.

Urey H. C. (1947) The thermodynamic properties of isotopic substances ed. S.-I. Karato. *J. Chem. Soc.*, 562.

Valdes M. C., Moreira M., Foriel J. and Moynier F. (2014) The nature of Earth's building blocks as revealed by calcium isotopes. *Earth Planet. Sci. Lett.* **394**, 135–145.

Vanderbilt D. (1990) Soft self-consistent pseudopotentials in a generalized eigenvalue formalism. *Phys. Rev. B* **41**, 7892–7895.

Wang W., Qin T., Zhou C., Huang S., Wu Z. and Huang F. (2017) Concentration effect on equilibrium fractionation of Mg-Ca isotopes in carbonate minerals: insights from first-principles calculations. *Geochim. Cosmochim. Acta* **208**, 185–197.

Wentzcovitch R. M. (1991) Invariant molecular-dynamics approach to structural phase transitions. *Phys. Rev. B* **44**, 2358–2361.

Wentzcovitch R. M., Yu Y. G. and Wu Z. (2010) Thermodynamic properties and phase relations in mantle minerals investigated by first principles quasiharmonic theory. *Rev. Mineral. Geochem.* **71**, 59–98.

Wu Z., Huang F. and Huang S. (2015) Isotope fractionation induced by phase transformation: first-principles investigation for Mg_2SiO_4. *Earth Planet. Sci. Lett.* **409**, 339–347.

Young E. D., Manning C. E., Schauble E. A., Shahar A., Macris C. A., Lazar C. and Jordan M. (2015) High-temperature equilibrium isotope fractionation of non-traditional stable isotopes: experiments, theory, and applications. *Chem. Geol.* **395**, 176–195.

Young E. D., Tonui E., Manning C. E., Schauble E. and Macris C. A. (2009) Spinel–olivine magnesium isotope thermometry in the mantle and implications for the Mg isotopic composition of Earth. *Earth Planet. Sci. Lett.* **288**, 524–533.

Zhao X., Zhang Z., Huang S., Liu Y., Li X. and Zhang H. (2017) Coupled extremely light Ca and Fe isotopes in peridotites. *Geochim. Cosmochim. Acta*.

Zhu P. and Douglas Macdougall J. (1998) Calcium isotopes in the marine environment and the oceanic calcium cycle. *Geochim. Cosmochim. Acta* **62**, 1691–1698.

Associate editor: Frederic Moynier